

Simplified mathematical model for calculating the oxygen excess ratio of a PEM fuel cell system in real-time applications

Abstract—The oxygen starvation phenomenon is a dangerous operating condition that reduces the lifetime of PEM fuel cells. The detection and prevention of this undesired phenomenon requires estimation of the oxygen excess ratio λ_{O_2} . The mathematical complexities of the reported methods for obtaining λ_{O_2} complicate its real-time calculation and require high-performance computational devices, which significantly increase the costs of the system. In this paper, a mutual information approach is used for obtaining a simplified mathematical model for the calculation of λ_{O_2} . The usage of such a simplified model requires much less computational power for real-time monitoring of the variable λ_{O_2} , while it provides comparable results to those obtained by using the complex model. Therefore it represents a cost-effective solution, suitable for usage within applications that require high sampling frequencies, like emulators, converter and air compressor control loops, simulations, etc. In order to validate the accuracy of this simplified λ_{O_2} calculation model, a real-time monitoring system was built and experimentally tested using both, the simplified and the complex model. The matching experimental results validate the proposed simplification and justify the use of this simplified model within real-time monitoring applications.

Index Terms—Fuel cell, oxygen starvation, mutual information, real-time system.

NOMENCLATURE

λ_{O_2}	Oxygen excess ratio [-].
$W_{O_2,ca,react}$	Oxygen flow rate [Kg/s].
$W_{O_2,ca,in}$	The mass flow rate of oxygen entering the cathode [Kg/s].
$x_{O_2,ca,in}$	Oxygen mass fraction [].
$y_{O_2,ca,in}$	Oxygen mole fraction entering the cathode, 0.21 [-].
$M_{a,ca,in}$	Molar mass of the dry air at the cathode inlet [].
$W_{a,ca,in}$	Mass flow rate of dry air entering the cathode [].
$W_{ca,in}$	Inlet air flow rate [Kg/s].
M_{am}	Inlet air molar mass [].
W_{cp}	Total mass flow rate provided by the compressor [].
x_v	Water-vapor fraction [].
p_{sat}	Saturation pressure [].
T	Stack temperature [K].
$\omega_{ca,in}$	Humidity ratio [].
$p_{ca,in}$	inlet pressure at the cathode [].
M_{O_2}	Oxygen molar mass, 32×10^{-3} [kg/mol].
n	Number of cells of the fuel cell stack, 46 [-].
F	Faraday constant, 96.487 [kC/mol].
M_{N_2}	Nitrogen molar mass, 28×10^{-3} [kg/mol].

M_v	Vapor molar mass, 18.02×10^{-3} [kg/mol].
$\phi_{ca,in}$	Inlet air relative humidity in the cathode, 1 [-].

I. INTRODUCTION

Power systems based on proton-exchange membrane fuel cell (PEMFC) technology have been the object of increasing attention and extensive research over recent years. PEMFCs, used as either main or auxiliary power sources, display a lot of potential for usages within both stationary and mobile applications. This is due to their high-efficiency, high-power density, fast start-up, low corrosion rate, low operating temperatures, solid electrolytes, non-polluting emissions into the environment, and longer cell as well as stack lifetimes in comparison with other kinds of fuel cells [1]–[3]. On the other hand, the relatively short lifespans of fuel cells represent a significant barrier for their commercialization in both stationary and mobile applications [4]–[6]. Therefore, a significant part of research about fuel cells focuses on prolonging their operational lives.

A phenomenon that may occur during load transients and reduce the lifetime of a fuel cell is known as “oxygen starvation” [3]. Four different approaches to studying this phenomenon can be found in the literature. The first approach is based on the development of mathematical models for studying oxygen starvation [7], [8]. These models estimate the oxygen excess ratio λ_{O_2} , which is the ratio between the oxygen supplied to the cathode channel and the oxygen consumed by the electrochemical reaction in the fuel cell. The main drawback of these models is their mathematical complexity that makes them unsuitable for real-time implementations within low-cost processors. The second approach uses mathematical oxygen excess ratio models, obtained using the first approach, for the development of realtime [emulation](#) systems [9], [10]. The main disadvantage of these simulation systems with λ_{O_2} estimation is their high economic cost. Further, these systems cannot be used within mobile applications because of their large sizes and weights. The third approach focuses on the air flow rate control as a way of preventing oxygen starvation [11]–[13]. Different control strategies for controlling the air compressor, like feed-forward control [7], [14], LQR [7], linear quadratic Gaussian (LQG) control [15], and model predictive control (MPC) [16], were proposed and tested using simulation. For experimental validation, it is necessary to use a control-oriented model that reduces the mathematical complexities of the simulation models. Hence, different MPCs were studied and developed in [17]–[20]. The main drawback of all MPC

strategies is that they control the air compressor, the response of which may be much slower than the variations in the current load. Thus, it is impossible to avoid peaks in the oxygen excess ratio after load transients, which can lead to the appearance of oxygen starvation phenomena. **One possible solution for these peaks within the oxygen excess ratio is to replace the conventional fuel cell air compressor for a switched reluctance motor that improve the time response and it is widely-used in high-speed applications [21].** Oxygen starvation can also be avoided by using batteries, ultracapacitors or other auxiliary power sources for supporting the operation of the FC, and thus ensure a fast response to any load power transient. The systems formed by a FC and another auxiliary power source, known as FC hybrid systems, have been a topic of extensive research over recent years [22]–[25]. These hybrid systems can limit the slope of the current or the power generated by the FC by using current-controlled dc-dc converters. Thus, the oxygen starvation phenomenon can be avoided and the system can operate with higher efficiency [26]–[29]. **However, this methodology is not appropriate since it is a very conservative strategy that penalizes the size of the auxiliary energy storage elements.**

Based on the aforementioned facts, the fourth approach for studying and avoiding the occurrence of oxygen starvation is related to the design of power converters. Although there are several converters that are designed exclusively for use within fuel cell applications [30]–[39], there are only a few applications in which the λ_{O_2} calculation is included within the converter's control or utilized for adjusting the converter's controller [10], [29]. This is due to the high complexities of the models used for estimating λ_{O_2} , which makes it impossible to calculate the instantaneous value of λ_{O_2} at a frequency near to the converter's switching frequency.

All the above-described methods may perform well in practice and thus serve their intentions, but they have a common drawback, which is the high complexity of the models for calculating the oxygen excess ratio. Complex models represent a serious obstacle to a wider usage of these methods in practice, since high-performance and consequently high-cost devices are needed for their implementation. While simplicity of the model is crucial for real-time implementation in a low-cost processor, the accuracy of the model is also important for the performance quality and the protection of the fuel cell. It can be inferred that both, the simplicity and the accuracy of the models, play important roles in the commercialization of oxygen starvation protection **tools**. Therefore, the aim of this work was to simplify these models for estimating λ_{O_2} , but not at the expense of degrading accuracy and performance.

A reduction in the order of a λ_{O_2} estimation model was achieved by using the mutual information (MI) approach. This methodology has been described and successfully applied for selection of variables from the initial set in spectrometric nonlinear modeling [40]. Thus, a new simplified mathematical model has been created for the calculation of λ_{O_2} with comparable performance and accuracy to the original one. The proposed simplified model can be easily implemented within emulators, converter control loops, air compressor control loops or simulations.

The remainder of this paper is organized as follows: Section II describes a conventional method for estimating the oxygen excess ratio, Section III presents a detailed description of the experimentally tested fuel cell system, and Section IV describes the proposed simplified model for estimating the oxygen excess ratio, obtained by using the MI method. Finally, the last two sections present the experimental results and conclusions of this work, respectively.

II. STANDARD OXYGEN EXCESS RATIO ESTIMATION

The ratio of air flow through the compressor to the cathode and the air required by the fuel cell achieving the reaction



in accordance with the demand of the load current, is normally expressed by the oxygen excess ratio λ_{O_2} [3], [8], that is

$$\lambda_{O_2} = \frac{W_{O_2,ca,in}}{W_{O_2,ca,react}}. \quad (2)$$

In order to avoid the oxygen starvation phenomenon, the oxygen excess ratio must be greater than 1 ($\lambda_{O_2} \geq 1$) [3], [8]. The oxygen flow rate during the fuel cell reaction is proportional to the stack current I_{st} , and can be calculated using electrochemical principles as

$$W_{O_2,ca,react} = M_{O_2} \frac{n \cdot I_{st}}{4F}. \quad (3)$$

The mass flow rate of oxygen entering the cathode $W_{O_2,in}$, presented in (2), can be calculated by

$$W_{O_2,ca,in} = x_{O_2,ca,in} \cdot W_{a,ca,in}, \quad (4)$$

where $x_{O_2,ca,in}$ is the oxygen mass fraction, which is a function of the oxygen mole fraction $y_{O_2,ca,in}$. The oxygen mass fraction is expressed as

$$x_{O_2,ca,in} = \frac{y_{O_2,ca,in} \cdot M_{O_2}}{M_{a,ca,in}}, \quad (5)$$

where $M_{a,ca,in}$ is the molar mass of the dry air at the cathode inlet, which can be calculated as

$$M_{a,ca,in} = y_{O_2,ca,in} \cdot M_{O_2} + (1 - y_{O_2,ca,in}) \cdot M_{N_2}. \quad (6)$$

The mass flow rate of dry air entering the cathode $W_{a,ca,in}$, presented in (4), is calculated as

$$W_{a,ca,in} = \frac{1}{1 + \omega_{ca,in}} \cdot W_{ca,in}, \quad (7)$$

where the inlet air flow rate $W_{ca,in}$ supplied by the compressor, in kilograms per second, can be calculated from

$$W_{ca,in} = \frac{W_{cp}}{22.4 \times 60} \cdot M_{am}, \quad (8)$$

where M_{am} is the inlet air molar mass and W_{cp} is the total mass flow rate provided by the compressor. In (8), W_{cp} is converted from the SLPM value obtained from the air compressor sensor, to kilograms per second as required in (7). The inlet air molar mass M_{am} used in (8) can be calculated as

$$M_{am} = (1 - x_v) \cdot M_{a,ca,in} + x_v \cdot M_v, \quad (9)$$

where the water-vapor fraction x_v in the inlet air can be expressed as [8]

$$x_v = \frac{\phi_{ca,in} \cdot p_{sat}}{1 - \phi_{ca,in} \cdot p_{sat}}. \quad (10)$$

The saturation pressure p_{sat} depends on the stack temperature T , expressed in Kelvin and is obtained from a thermodynamic table of vapor [7] as

$$\log_{10}(p_{sat}) = (-1.69 \times 10^{-10}) \cdot T^4 + (3.85 \times 10^{-7}) \cdot T^3 + (-3.39 \times 10^{-4}) \cdot T^2 + 0.143 \cdot T - 20.92. \quad (11)$$

Returning to equation (7), it is necessary to define the humidity ratio, which can be expressed as

$$\omega_{ca,in} = \frac{M_v}{M_{a,ca,in}} \cdot \frac{\phi_{ca,in} \cdot p_{sat}}{p_{ca,in} - \phi_{ca,in} \cdot p_{sat}}, \quad (12)$$

where $p_{ca,in}$ is the inlet pressure at the cathode. This variable is very difficult to measure due to the closed construction of the fuel cell system. Therefore, a simplified model of the cathode inlet pressure, identified by simulation, was proposed in [17] as follows

$$p_{ca,in} \approx 1.0033 + 2.1 \times 10^{-3} \cdot W_{cp} - 475.7 \times 10^{-6} \cdot I_{st}. \quad (13)$$

For the calculation of λ_{O_2} , it is necessary to acquire the fuel cell temperature T , the total mass flow rate provided by the compressor W_{cp} , and the stack current I_{st} . In most past studies about the oxygen excess ratio, the fuel cell temperature T was assumed to be constant at a value equal to the ambient temperature [17]–[20], while some other works proposed a complex thermal model that is difficult to implement within a real-time application [8]. The stack current I_{st} is calculated by summing the measured current through the load I_{load} and the estimated value of the fuel cell's auxiliary equipment current I_{aux} [8], [17]. The next section presents the way in which the variables (T , I_{st} , W_{cp}) necessary for the calculation of λ_{O_2} , were sensed and characterized.

III. FUEL CELL SYSTEM DESCRIPTION

This work was performed using the Nexa PEMFC from Ballard. Presently, this fuel cell remains a world benchmark since it has been widely used by different research groups and represents the state of the art in terms of PEM technology [17]. However, the results presented in this paper can be extended to other types of PEM fuel cells. The Nexa fuel cell is a fully integrated system that produces unregulated

DC power, up to 1.2 kW, from a supply of hydrogen and air. The Nexa power module comes with LabVIEW software, which provides a graphical user interface to the Nexa modules operational status and performance [41]. This software monitors the key process parameters of the fuel cell and can generate a data-logging file with the following parameters: stack temperature, stack voltage, stack current, fuel pressure, fuel leak, fuel consumption, oxygen concentration, ambient air temperature, purge cell voltage, battery voltage (used to start the power module), process air flow, air pump operating voltage, hydrogen concentration bridge voltage, process air pump duty-cycle, and cooling air fan duty-cycle. A serial port is used to communicate the mentioned variables from the fuel cell to the LabVIEW software using the RS-232 communication standard, hence its high sampling time of 200 ms. However, the data that is monitored by the FC software can not be acquired in real-time for characterizing the sensors required (T , I_{st} , W_{cp}) for the calculation of λ_{O_2} . Therefore, it was necessary to develop a LabVIEW program for reading the measurements in real-time from the serial port and to compare them with the measurements from the sensors using an acquisition card PCI6024E of National Instruments. Through this program and the measured values obtained from the already installed sensors within the Nexa FC, it was possible to characterize the mass flow rate W_{cp} and temperature sensor T of the fuel cell, as shown in Figs. 1 and 2. The relation between the compressor total mass flow rate W_{cp} and the voltage of the sensor V_{wcp} is presented in (14). In the same way, the relation between the fuel cell temperature T and the voltage of the sensor V_T is given in (15). Both sensor characteristics were identified using the MATLAB curve fitting toolbox.

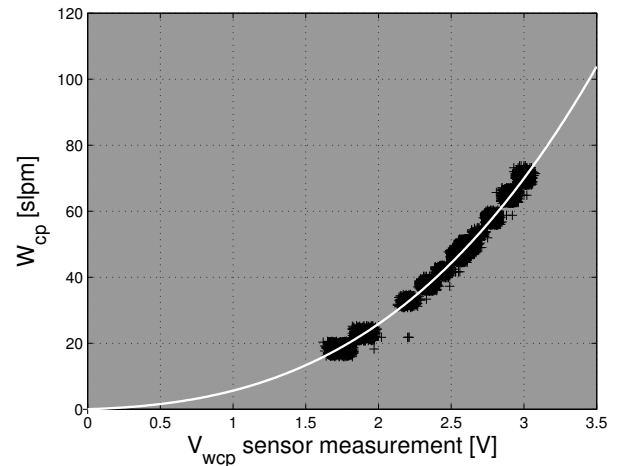


Fig. 1. Static characteristic that presents a nonlinear behaviour between the total mass flow rate provided by the compressor W_{cp} and the sensor measurements presented by black plus. The identified characteristic curve that corresponds to (14) is presented by a white solid line.

$$W_{cp} = 1.551 \cdot V_{wcp}^3 + 2.632 \cdot V_{wcp}^2 + 1.452 \cdot V_{wcp} \quad (14)$$

$$T = 6.222 \cdot V_T^3 - 53.16 \cdot V_T^2 + 169.5 \cdot V_T - 161.9 \quad (15)$$

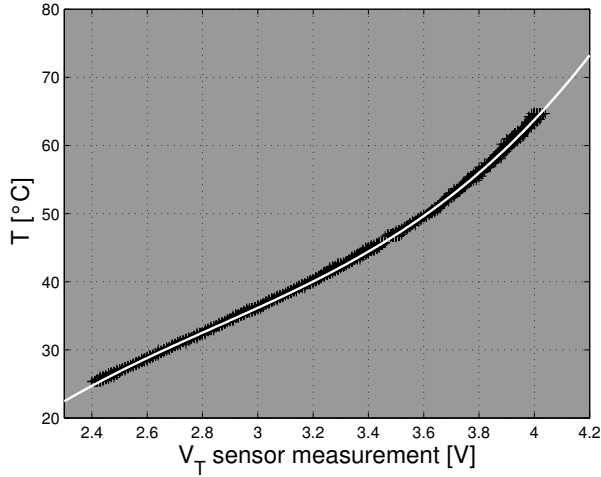


Fig. 2. Static characteristic that presents a nonlinear behaviour between the fuel cell temperature and the sensor measurement presented by black plus. The white solid line is the identified characteristic curve that corresponds to (15).

The remaining variable for calculating λ_{O_2} is the current generated by the FC stack I_{st} , which is used for feeding the auxiliary equipment necessary for the correct operation of the FC and the load connected to the FC. It can be defined as

$$I_{st} = I_{aux} + I_{load}, \quad (16)$$

where I_{aux} is the current that feeds the auxiliary equipment, and I_{load} the load current. In order to determine the stack current I_{st} on the basis of (16), current sensors were installed at the load connection point and within the auxiliary equipment of the FC system. The use of these sensors reduces the complexity of the mathematical model, since the estimation of I_{aux} is avoided [8], [17].

IV. SIMPLIFIED OXYGEN EXCESS RATIO ESTIMATION

A. Mutual Information Estimation using K-nearest neighbors

In this paper, mutual information is used as a criterion for selecting the most relevant variables for the prediction of λ_{O_2} behavior. Given a multiple input single output (MISO) function approximation problem, with input variables $X = [x_1, x_2, \dots, x_n]$ and output variable $Y = y$, the main goal of MI is to measure the dependence between random variables. In the actual case, the input variables are the key process parameters of the fuel cell, monitored by Nexa software, and the output variable is the standard oxygen excess ratio estimation using (2). The mutual information between two continuous random variables X and Y is defined as

$$I(X, Y) = \int p_{X,Y}(x, y) \log \frac{p_{X,Y}(x, y)}{p_X(x)p_Y(y)} dx dy \quad (17)$$

where $p_{X,Y}(x, y)$ is a joint density function, and $p_X(x)$ and $p_Y(y)$ are the marginal density functions, respectively.

Estimation of the mutual information from equation (17) requires prior estimation of $p_{X,Y}(x, y)$. Several approaches have been proposed for the estimation of $p_{X,Y}(x, y)$, such

as histograms and kernel density estimation [42]. They both suffer from the curse of dimensionality [40]. For this reason, a k -NN based density estimation is used. The k -NN approach uses a fixed number k of nearest neighbors to estimate the MI. In practice, one has at one's disposal a set of N input-output pairs which form the points within the data set. The minimum volume that encompasses k points is determined for each point within the data set. The MI can be estimated by counting the number of points inside this volume in the marginal spaces [43]. The mutual information is estimated as

$$\hat{I}(X, Y) = \psi(k) - \frac{1}{k} - \frac{1}{N} \sum_{i=1}^N [\psi(n_x^i) + \psi(n_y^i)] + \psi(N) \quad (18)$$

where n_x^i and n_y^i are the neighbors of the i -th data point in the x and y dimensions, respectively, and ψ is the digamma function given by

$$\psi(t) = \frac{\Gamma'(t)}{\Gamma(t)} = \frac{d}{dt} \ln \Gamma(t) \quad (19)$$

with

$$\Gamma(t) = \int_0^{\infty} u^{t-1} e^{-u} du. \quad (20)$$

The quality of the estimator $\hat{I}(X, Y)$ is related to the chosen value for k . A value of $k = 6$ is set as suggested in [44].

B. Variable selection

The estimator $\hat{I}(X, Y)$, defined in (18), is used to select a subset of variables, which contribute to predicting the output Y , from input variables X_j with $j = 1, \dots, M$. As any subset of the input variables can be selected, the optimal algorithm would be to calculate MI for every possible subset and to select the subset with the highest MI.

1) *Selection of the first variable:* The first variable to be chosen from the set X_j is the one that maximizes the mutual information with Y :

$$X_{s1} = \operatorname{argmax}_{X_j} \left\{ \hat{I}(X_j, Y) \right\}, \quad 1 \leq j \leq M,$$

where X_{s1} denotes the first selected variable. Using the same notation as before, subsequently selected variables will be denoted $X_{s2}, X_{s3}, \dots, X_{sM}$.

C. Forward selection

Forward selection is the procedure for selecting the next variables. When selecting the second variable it has to be taken into account that variable X_{s1} has already been selected. Thus, X_{s2} is the one that maximizes the mutual information between the set $\{X_{s1}, X_{s2}\}$ and the output variable Y :

$$X_{s2} = \operatorname{argmax}_{X_j} \left\{ \hat{I}(\{X_{s1}, X_j\}, Y) \right\}, \quad 1 \leq j \leq M, j \neq s1$$

In this sense, the t -th selected variable X_{st} will be chosen according to

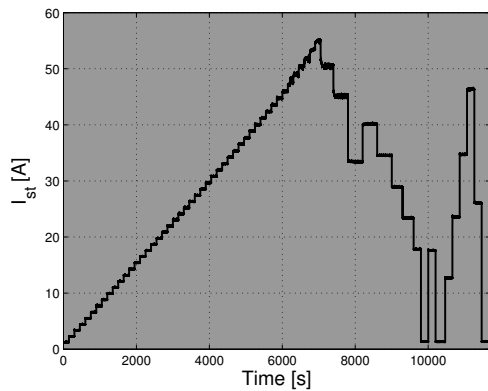
$$X_{st} = \operatorname{argmax}_{X_j} \left\{ \hat{I}(\{X_{s1}, X_{s2}, \dots, X_{s(t-1)}, X_j\}, Y) \right\}, \quad 1 \leq j \leq M, j \neq \{s1, s2, \dots, s(t-1)\}$$

D. Stopping criterion

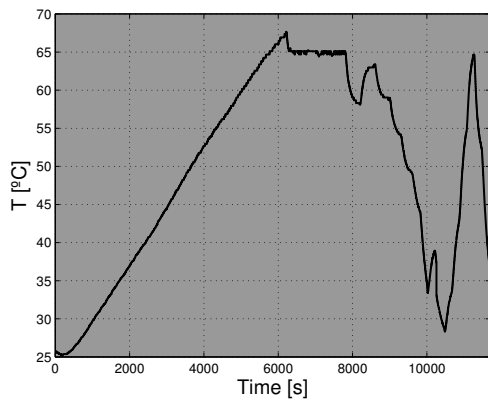
The forward selection procedure is considered as a ranking algorithm, since the selected variables are ordered according to their mutual information with the output [40]. This procedure is stopped in those cases where MI decreases after a forward step. For the example

$$\hat{I}(\{X_{s1}, \dots, X_{s(t)}\}, Y) > \hat{I}(\{X_{s1}, \dots, X_{s(t+1)}\}, Y)$$

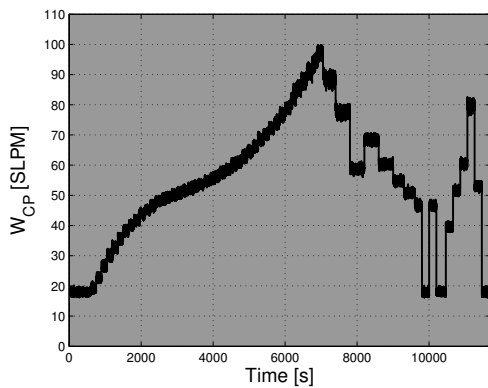
the procedure is stopped at step t .



(a)



(b)



(c)

Fig. 3. Experimental profiles of the variables required for the model's validation: (a) stack current I_{st} , (b) fuel cell temperature T_{st} , (c) total mass flow rate W_{cp} .

E. Input variable selection for $\hat{\lambda}_{O_2}$ calculation

The MI estimation was applied to the fuel cell's experimental measurement data, in order to determine which of the Nexa FC sensors have greater influence on the value of the oxygen excess ratio variable. An experiment had to be carried out in order to acquire the required measurement data from all the installed Nexa FC's sensors. During that experiment, the FC had to operate at various operational points with severe transients between them. In order to achieve such testing conditions, the FC current profile shown in Fig. 3(a) was generated using an electronic load. The information from all the FC's sensors, described in Section III, was monitored and stored by the Nexa software each 200 ms. The data acquired from the sensors was used to form the variable X , which represented the multiple input variable for the MI estimation. The recorded values of the sensors for T , I_{st} , and W_{cp} , as shown in Fig. 3, were used for calculating the oxygen excess ratio λ_{O_2} , which was calculated according to the standard procedure, as presented in Section II. The calculated values of λ_{O_2} were then used to form the single output variable Y for the MI estimation procedure. Finally, the MI estimation was carried out on variables X and Y . The results are shown in Table II, where the observed variables are sorted according to their influence on the behavior of the oxygen excess ratio from the most to the least relevant.

TABLE I
VARIABLES' RANKINGS FOR λ_{O_2} .

Rank	1	2
Variable	W_{cp}	I_{st}

Table IV-E shows that the most relevant variables are W_{cp} and I_{st} . W_{cp} and I_{st} are related to the numerator and denominator of (2), respectively. In order to avoid a non-linear regression model, linear dependence was tested between the variables $W_{O_2,ca,in}$ and W_{cp} , and $W_{O_2,ca,react}$ and I_{st} . The linear dependence test results are given in Figs. 4 and 5. Both figures present a high correlation between the observed data, indicating a linear relation between the variables.

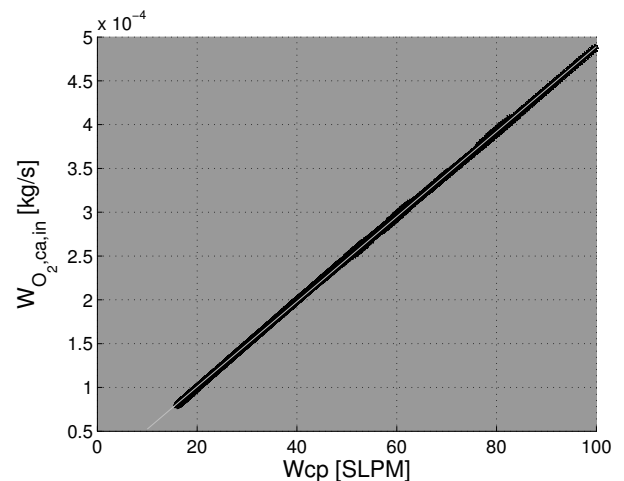


Fig. 4. Linear regression between $W_{O_2,ca,in}$ and W_{cp} .

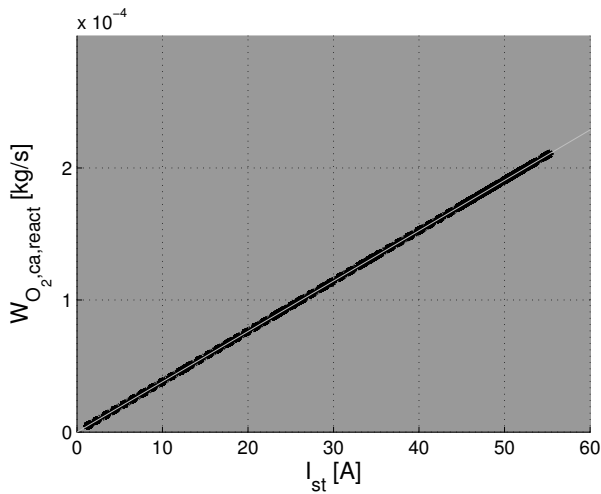


Fig. 5. Linear regression between $W_{O_2,ca,react}$ and I_{st} .

From the linear regressions shown in Figs. 4 and 5, the following relations were obtained

$$W_{O_2,ca,in} \approx 4.98 \times 10^{-6} \frac{\text{kg}}{\text{s} \cdot \text{SLPM}} \cdot W_{cp}, \quad (21)$$

$$W_{O_2,ca,react} \approx 3.81 \times 10^{-6} \frac{\text{kg}}{\text{s} \cdot \text{A}} \cdot I_{st}. \quad (22)$$

Another way to obtain the equations (21) and (22) is through a knowledge of the classical model presented in Section II and the performing modeling approaches. Therefore, $W_{O_2,ca,react}$ is calculated by substituting the numeric values of M_{O_2} , n and F in (3), which yields (22). On the other hand, the numerator term, $W_{O_2,ca,in}$ given in (4), is obtained by applying (5) and (6) and taking into account that the air to the cathode is humidified, therefore the humidity ratio is equal to zero. After substituting the numeric values the expression (21) is obtained. However, the goal of the MI estimation was to determine which of the 15 FC variables have greater influence on the λ_{O_2} calculation and it was an independent estimation of the of the classical model presented in Section II. Hence, it was presented an alternative way to obtain the equations (21) and (22) without prior knowledge of the classical model.

From (21) and (22), λ_{O_2} could be approximated by

$$\hat{\lambda}_{O_2} \approx 1.31 \frac{\text{A}}{\text{SLPM}} \times \frac{W_{cp}}{I_{st}}, \quad (23)$$

where $\hat{\lambda}_{O_2}$ is the approximated oxygen excess ratio that could be obtained from a simplified model.

The most significant advantage of the simplified model is that it is represented by one simple equation (23), while the complex model consists of a set of equations, as presented in Section II. It must also be noted that calculating $\hat{\lambda}_{O_2}$ using the simplified model (23) does not require information about the FC temperature. This is another advantage over the standard calculation method, presented in Section II. Although it is well known that the FC temperature T is a slow dynamic variable in comparison with the total mass flow rate provided by the compressor W_{cp} and the stack current

I_{st} . However, it was performance a long duration experiments that obtained large-signal FC temperature T variations in all the operation range as shown in Fig. 3(b). So it was not obvious to make a temperature model simplification of the classic methodology to obtain the final result presented in (23). This was hence one of the most significant contributions of the MI estimation. The proposed simplified model represents a significant mathematical simplification of the standard model for calculating the oxygen excess ratio. Its use can significantly speed-up simulations and it can be implemented within the low-cost processors used in various real-time applications, like monitoring, converter control, and air compressor control.

Finally, a comparison between λ_{O_2} , obtained from the complex model and $\hat{\lambda}_{O_2}$, obtained from the simplified model, is presented in Fig. 6. The test was performed at the current profile shown in Fig. 3(a). A mean square error value of 0.0259 indicated that the results obtained by the simplified model with the sampling time of 200 ms, adequately matched the results obtained from using the complex model.

V. EXPERIMENTAL RESULTS

The previous section showed that the simplified model for calculating $\hat{\lambda}_{O_2}$ is a good approximation for the standard estimation of λ_{O_2} at the maximum sampling time of 200 ms that can be achieved by the Nexa monitoring software. In the next step, the validity of the proposed model had to be proven for smaller sampling times. This could only be achieved by acquiring the instantaneous values of key variables directly from the fuel cell, due to the 200 ms sampling time limitation imposed by the serial communication. In order to achieve sampling times below 200 ms and thus overcome the limitations of the Nexa monitoring software, a low-cost real-time oxygen excess ratio monitoring system was designed and built. This monitoring device is shown in Fig. 7, while its block diagram and connection scheme with the FC system and the load are illustrated in Fig. 8. The device in Fig. 7 represents the first real-time oxygen excess ratio monitoring system designed exclusively for FC applications that can be found within scientific literature or commercial applications. The main advantages and features of the developed system are: the use of a low-cost dsPIC microcontroller that enables real-time calculations, a keypad that allows full system configuration and adaptation to various types of FCs, oxygen starvation indication, visualization of the main variables within the LCD display, data storage within an external USB memory, an analog output signal port for observing signals with an oscilloscope or using them as feedback for control, additional channels for future applications (digital input/output channels, analog output channels and PWM output channels), no need for external power supply and low power consumption. In addition, other advantage of the real-time oxygen excess ratio monitoring system is its low cost which represents a 0.5% of the Nexa fuel cell price according with [45]. The discussed monitoring device can be used in both static and mobile applications, since it is compact, lightweight, and easily portable.

The real-time oxygen excess ratio monitoring system is programmed to perform the calculation of λ_{O_2} using (2) and

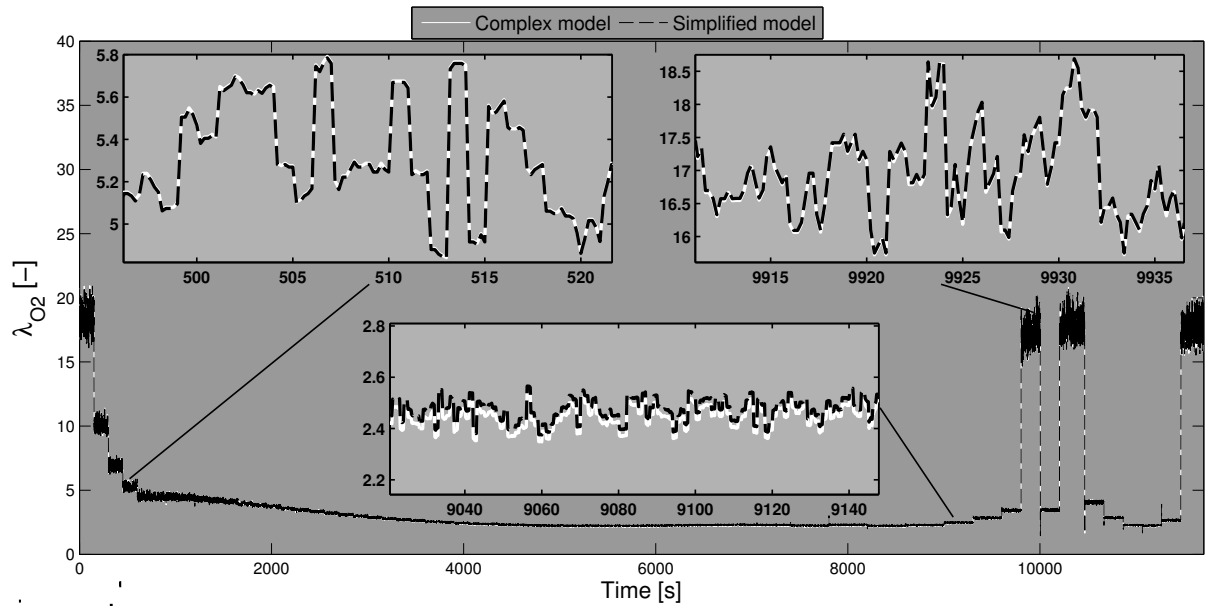


Fig. 6. Comparison between λ_{O_2} calculated using (2) and $\hat{\lambda}_{O_2}$ approximated by means of (23), by the experimental profile presented in Fig. 3.

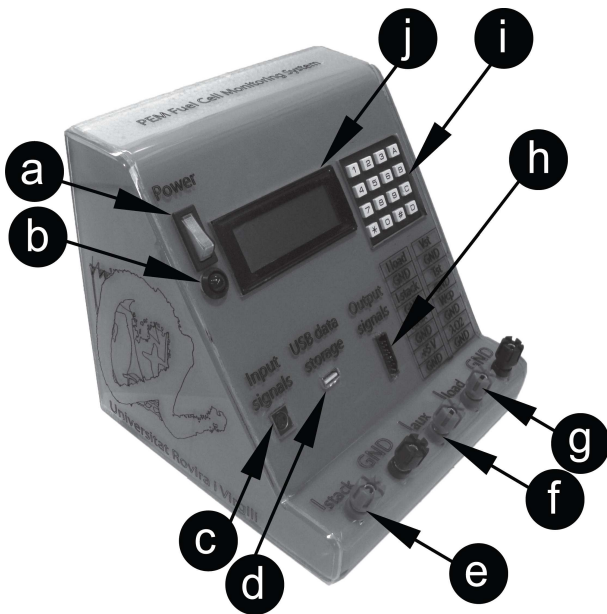


Fig. 7. Real-time oxygen excess ratio monitoring system: (a) on-off switch, (b) oxygen starvation alarm (c) input signals (T and W_{cp}) (d) USB data storage, (e) I_{st} connector, (f) I_{aux} connector, (g) I_{load} connector, (h) output signals connector in a range of 0 to 4 V (I_{load} , I_{st} , I_{aux} , V_{st} , T , W_{cp} , λ_{O_2}) and +5 V and ground to supply external circuits, (i) keypad for user interaction, (j) LCD displays the main variables (λ_{O_2} , V_{st} , I_{st} and T).

$\hat{\lambda}_{O_2}$ using (23) every 1 ms. This represents a 200 times reduction of the smallest sampling time that can be achieved by the Nexa software. The 1 ms sampling time of the proposed real-time oxygen excess ratio monitoring system is limited by the complexity of λ_{O_2} calculation. However, it is possible to achieve sampling times down to 200 μs , in the case of calculating only $\hat{\lambda}_{O_2}$. Fig. 9 shows the behavior of the oxygen excess ratio for a 10 A sudden increase of the load current. It is evident from this figure that the oxygen excess ratio

$\hat{\lambda}_{O_2}$ obtained by the simplified calculation, matches with λ_{O_2} obtained by the standard calculation method. The same can be concluded for the results shown in Fig. 10, which were recorded for a 10 A abrupt decrease of the load current. Fig. 10 also shows that right after the load current decreases, the oxygen excess ratio rises to values above $\lambda_{O_2} = \hat{\lambda}_{O_2} = 8$. These values are out of range for the proposed monitoring device due to the 4 V output voltage limitation of the used digital-to-analog converters, but do not affect the oxygen starvation study, since the aim is detect when the oxygen excess ratio falls under the value of 1. It can be seen from both figures that the total mass flow rate provided by the compressor W_{cp} reaches its steady state value in 400 ms for a load current increase of 10 A and in 600 ms for a load current decrease of 10 A. In [17], the authors used an acquisition card with a sampling time of 10 ms for acquiring the measurement data from the sensor of W_{cp} . They concluded that W_{cp} reaches the steady state in less than 10 ms after an abrupt load change, which is in contradiction with the experimental results shown in Figs. 9 and 10.

The aim of the final experiment was to test the monitoring device at the full computational power of the used microcontroller. In order to achieve this, only the simplified mathematical model for the calculation of $\hat{\lambda}_{O_2}$ was implemented within the processor. A load current profile that simulates different operation points and transient states was generated for testing purposes. The results of the experiment are shown in Fig. 11. It can be seen from the zoomed-in part of the figure, that a load current increase of 30 A pushes the fuel cell into the harmful phenomenon of oxygen starvation. The noise in the signals in Fig. 11 is due to the auxiliary systems of the fuel cell, especially the air compressor and the cooling motor. This was detected and verified by independent measurements of the connections with auxiliary equipment. Either analog or digital filters can be used for mitigation of that noise. They have to

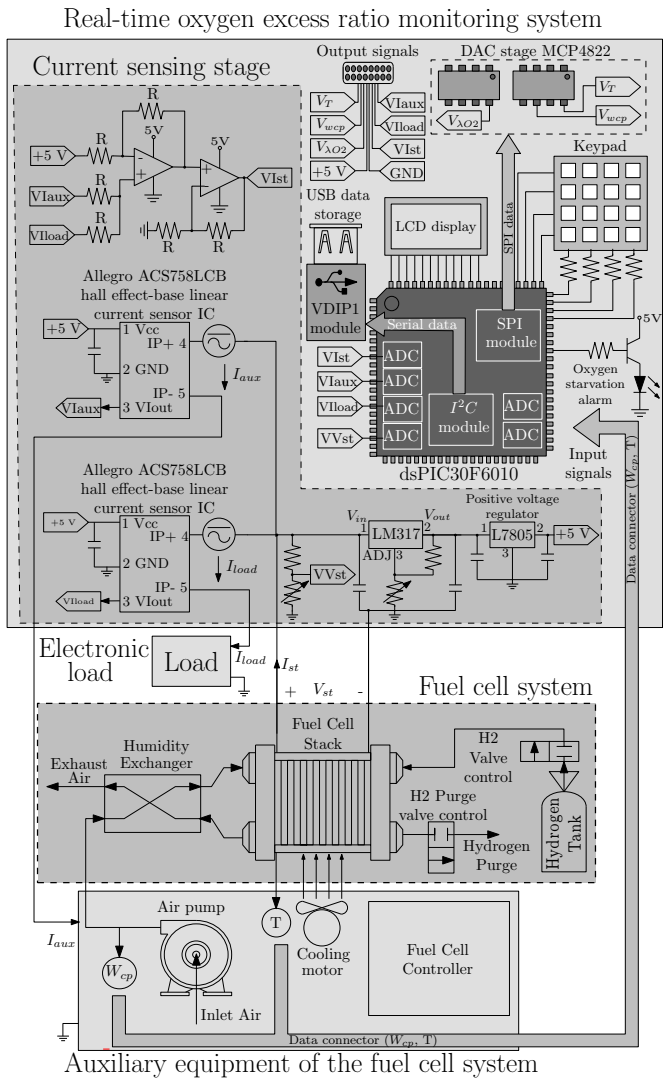


Fig. 8. Real-time oxygen excess ratio monitoring block diagram, which presents the connections with the fuel cell system and the load.

be designed according to the requirements of the application for which the monitoring system is used. The design of such filters exceeds the framework of this research. However, the most important feature of the proposed oxygen excess ratio estimation system is that it ensures high computational power, which is crucial for successful integration and good performance of the device within various fuel cell applications.

VI. CONCLUSION

A simplified mathematical model for calculating the oxygen excess ratio of a PEM fuel cell was obtained by using the mutual information approach. The proposed simplified model exhibited the same behavior as the complex model during experiments made using a purpose-built real-time monitoring system connected to the Nexa PEM fuel cell. The main advantage of the new model is in providing much faster calculation of the oxygen excess ratio, while achieving analogous results, in comparison with the conventional complex model. Experimental tests using a dsPIC30F6010 processor showed that the classical model was able to calculate a new λ_{O_2} value

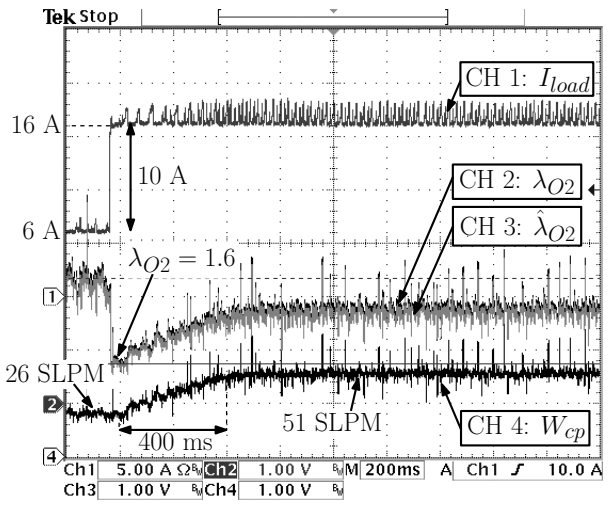


Fig. 9. Oxygen excess ratio behavior for a load current increase of 10 A. I_{load} (5 A/div), λ_{O_2} (2/div), $\dot{\lambda}_{O_2}$ (2/div) and W_{cp} (31.86 SLPM/div).

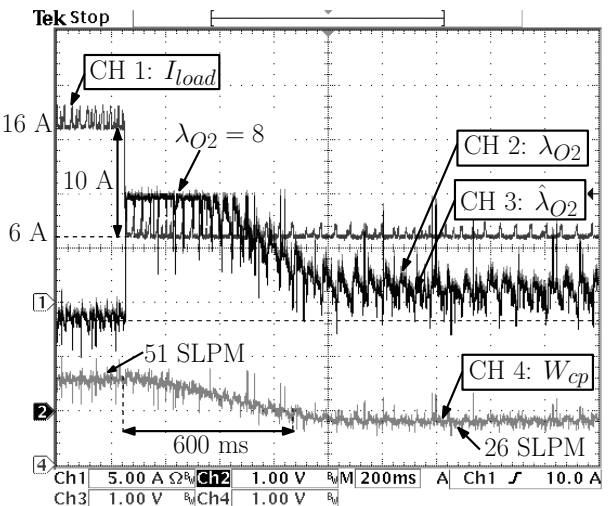


Fig. 10. Oxygen excess ratio behavior for a load current decrease of 10 A. I_{load} (5 A/div), λ_{O_2} (2/div), $\dot{\lambda}_{O_2}$ (2/div) and W_{cp} (31.86 SLPM/div).

each 1 ms, while the simplified model returned a new value every 200 μ s. Since λ_{O_2} is a good indicator of the harmful oxygen starvation phenomenon, the duration of its computation cycle and the accuracy of the result represent determinant factors for those processes used for the protection and lifetime extension of PEM fuel cells. One application, where the use of a simplified model can be proven as beneficial, are simulations on the system level, the total simulation time of which can be significantly reduced when using the proposed simplified model. In practical applications, the advantage of the simplified model is mainly in the possibility of implementing it within a low cost processor and integrating the oxygen excess ratio monitoring system into the control of a switching power converter, in order to limit the fuel cell's output current, and thus prevent any occurrence of the oxygen starvation phenomenon.

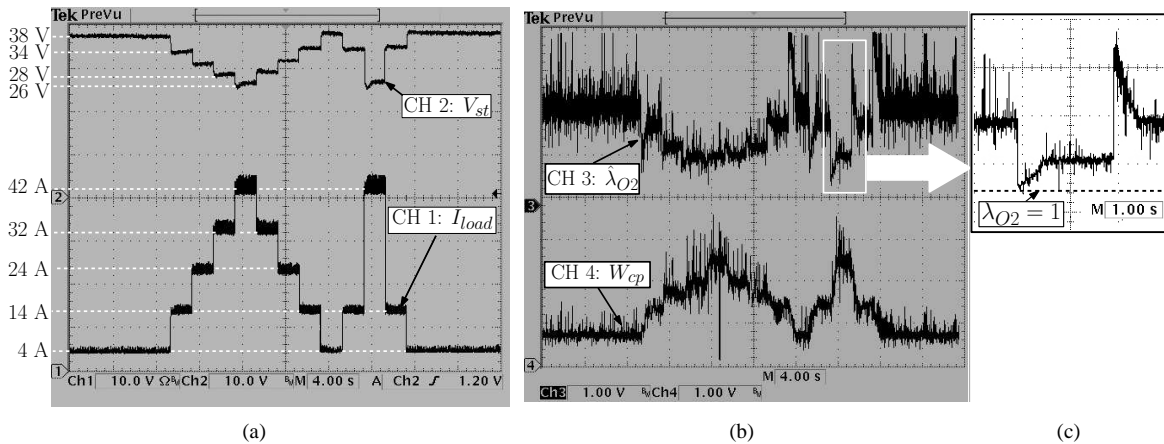


Fig. 11. Oxygen excess ratio behavior for a load profile with step-like transitions. I_{load} (10 A/div), V_{st} (10 V/div), $\hat{\lambda}_{O_2}$ (2/div) and W_{cp} (31.86 SLPM/div).

REFERENCES

- [1] J. Larminie and A. Dicks, *Fuel Cell Systems Explained*, 2nd ed. Publisher Wiley, 2003.
- [2] J. Correa, F. Farret, L. Canha, and M. Simoes, "An electrochemical-based fuel-cell model suitable for electrical engineering automation approach," *IEEE Trans. Ind. Electron.*, vol. 51, no. 5, pp. 1103 – 1112, oct. 2004.
- [3] J. Pukrushpan, A. Stefanopoulou, and H. Peng, "Control of fuel cell breathing," *IEEE Control Syst. Mag.*, vol. 24, no. 2, pp. 30 – 46, apr 2004.
- [4] P. Thounthong and P. Sethakul, "Analysis of a fuel starvation phenomenon of a pem fuel cell," in *Power Convers. Conf., PCC*, April 2007, pp. 731–738.
- [5] D. Nelson, M. Nehrir, and V. Gerez, "Economic evaluation of grid-connected fuel-cell systems," *Energy Conversion, IEEE Transactions on*, vol. 20, no. 2, pp. 452 – 458, june 2005.
- [6] B. Wahdame, D. Candusso, X. Francois, F. Harel, M.-C. Pera, D. Hissel, and J. Kauffmann, "Analysis of a fuel cell durability test based on design of experiment approach," *Energy Conversion, IEEE Transactions on*, vol. 23, no. 4, pp. 1093 – 1104, dec. 2008.
- [7] H. P. Jay T. Pukrushpan, Anna G. Stefanopoulou, *Control of fuel cell power systems: principles, modeling, analysis, and feedback design*, 1st ed. Springer, 2004.
- [8] C. Ramos-Paja, R. Giral, L. Martinez-Salamero, J. Romano, A. Romero, and G. Spagnuolo, "A PEM fuel-cell model featuring oxygen-excess-ratio estimation and power-electronics interaction," *IEEE Trans. Ind. Electron.*, vol. 57, no. 6, pp. 1914 – 1924, june 2010.
- [9] J.-H. Jung, S. Ahmed, and P. Enjeti, "PEM Fuel-Cell stack model development for real-time simulation applications," *IEEE Trans. Ind. Electron.*, vol. 58, no. 9, pp. 4217 – 4231, sept. 2011.
- [10] C. Restrepo, C. Ramos-Paja, R. Giral, J. Calvente, and A. Romero, "Fuel cell emulator for oxygen excess ratio estimation on power electronics applications," *Computers and Electrical Engineering*, vol. 38, no. 4, pp. 926 – 937, 2012.
- [11] K.-W. Suh and A. Stefanopoulou, "Performance limitations of air flow control in power-autonomous fuel cell systems," *Control Systems Technology, IEEE Transactions on*, vol. 15, no. 3, pp. 465 – 473, may 2007.
- [12] R. Talj, D. Hissel, R. Ortega, M. Becherif, and M. Hilairet, "Experimental validation of a pem fuel-cell reduced-order model and a moto-compressor higher order sliding-mode control," *IEEE Trans. Ind. Electron.*, vol. 57, no. 6, pp. 1906 – 1913, june 2010.
- [13] F. Marignetti, M. Minutillo, A. Perna, and E. Jannelli, "Assessment of Fuel Cell performance under different air stoichiometries and fuel composition," *IEEE Trans. Ind. Electron.*, vol. 58, no. 6, pp. 2420 – 2426, june 2011.
- [14] J. Pukrushpan, A. Stefanopoulou, S. Varigonda, J. Eborn, and C. Haugstetter, "Control-oriented model of fuel processor for hydrogen generation in fuel cell applications," *Contr. Eng. Practice*, vol. 14, no. 3, pp. 277 – 293, 2006.
- [15] S. Rodatz, G. Paganelli, and L. Guzzella, "Optimizing air supply control of a PEM fuel cell system," in *American Control Conference, 2003. Proceedings of the 2003*, vol. 3, june 2003, pp. 2043–2048.
- [16] C. Bordons, A. Arce, and A. del Real, "Constrained predictive control strategies for PEM fuel cells," in *American Control Conference*, june 2006, pp. 2486–2491.
- [17] J. Gruber, M. Doll, and C. Bordons, "Design and experimental validation of a constrained mpc for the air feed of a fuel cell," *Contr. Eng. Practice*, vol. 17, no. 8, pp. 874 – 885, 2009.
- [18] W. Garcia-Gabin, F. Dorado, and C. Bordons, "Real-time implementation of a sliding mode controller for air supply on a PEM fuel cell," *Journal of Process Control*, vol. 20, no. 3, pp. 325 – 336, 2010.
- [19] A. Arce, A. del Real, C. Bordons, and D. Ramirez, "Real-time implementation of a constrained MPC for efficient airflow control in a PEM Fuel Cell," *IEEE Trans. Ind. Electron.*, vol. 57, no. 6, pp. 1892 – 1905, june 2010.
- [20] J. Gruber, C. Bordons, and A. Oliva, "Nonlinear MPC for the airflow in a PEM fuel cell using a Volterra series model," *Control Engineering Practice*, vol. 20, no. 2, pp. 205 – 217, 2012.
- [21] T. Raminoso, B. Blunier, D. Fodorean, and A. Miraoui, "Design and optimization of a switched reluctance motor driving a compressor for a PEM Fuel-Cell system for automotive applications," *IEEE Trans. Ind. Electron.*, vol. 57, no. 9, pp. 2988 – 2997, sept. 2010.
- [22] F. Segura, J. Andujar, and E. Duran, "Analog current control techniques for power control in PEM fuel-cell hybrid systems: A critical review and a practical application," *IEEE Trans. Ind. Electron.*, vol. 58, no. 4, pp. 1171 – 1184, april 2011.
- [23] M. Vasallo, J. Andujar, C. Garcia, and J. Brey, "A methodology for sizing backup fuel-cell/battery hybrid power systems," *IEEE Trans. Ind. Electron.*, vol. 57, no. 6, pp. 1964 – 1975, june 2010.
- [24] A. Shahin, M. Hinaje, J.-P. Martin, S. Pierfederici, S. Rael, and B. Davat, "High voltage ratio DC-DC converter for fuel-cell applications," *IEEE Trans. Ind. Electron.*, vol. 57, no. 12, pp. 3944 – 3955, dec. 2010.
- [25] X. Zhu, X. Li, G. Shen, and D. Xu, "Design of the dynamic power compensation for PEMFC distributed power system," *IEEE Trans. Ind. Electron.*, vol. 57, no. 6, pp. 1935 – 1944, june 2010.
- [26] P. Rodatz, G. Paganelli, A. Sciarretta, and L. Guzzella, "Optimal power management of an experimental fuel cell/supercapacitor-powered hybrid vehicle," *Control Engineering Practice*, vol. 13, no. 1, pp. 41 – 53, 2005.
- [27] P. Corbo, F. Corcione, F. Migliardini, and O. Veneri, "Experimental assessment of energy-management strategies in fuel-cell propulsion systems," *J. of Power Sources*, vol. 157, no. 2, pp. 799 – 808, 2006.
- [28] P. Thounthong, S. Rael, B. Davat, and I. Sadli, "A control strategy of fuel cell/battery hybrid power source for electric vehicle applications," in *Power Electronics Specialists Conference, 2006. PESC '06. 37th IEEE*, june 2006, pp. 1 – 7.
- [29] C. Ramos-Paja, C. Bordons, A. Romero, R. Giral, and L. Martinez-Salamero, "Minimum fuel consumption strategy for PEM fuel cells," *IEEE Trans. Ind. Electron.*, vol. 56, no. 3, pp. 685 – 696, 2009.
- [30] A. Rathore and U. Prasanna, "Novel snubberless bidirectional zcs/zvs current-fed half-bridge isolated dc/dc converter for fuel cell vehicles," in

- IECON 2011 - 37th Annual Conference on IEEE Industrial Electronics Society*, nov. 2011, pp. 3033–3038.
- [31] M. Kabalo, B. Blunier, D. Bouquain, M. Simoes, and A. Miraoui, "Modeling and control of 4-phase floating interleaving boost converter," in *IECON 2011 - 37th Annual Conference on IEEE Industrial Electronics Society*, nov. 2011, pp. 3026–3032.
- [32] S. Cheng, Y. Lo, H. Chiu, and S. Kuo, "High efficiency digital controlled interleaved power converter for high power PEM fuel cell applications," *IEEE Trans. Ind. Electron.*, vol. PP, no. 99, p. 1, 2012.
- [33] J.-Y. Lee, Y.-S. Jeong, and B.-M. Han, "A two-stage isolated/bidirectional DC/DC converter with current ripple reduction technique," *IEEE Trans. Ind. Electron.*, vol. 59, no. 1, pp. 644–646, jan. 2012.
- [34] A. Rathore, A. Bhat, and R. Oruganti, "Analysis, design and experimental results of wide range zvs active-clamped L-L type current-fed DC/DC converter for fuel cells to utility interface," *IEEE Trans. Ind. Electron.*, vol. 59, no. 1, pp. 473–485, jan. 2012.
- [35] B. Yuan, X. Yang, X. Zeng, J. Duan, J. Zhai, and D. Li, "Analysis and design of a high step-up current-fed multiresonant DC-DC converter with low circulating energy and zero-current switching for all active switches," *IEEE Trans. Ind. Electron.*, vol. 59, no. 2, pp. 964–978, feb. 2012.
- [36] R. Andersen and I. Barbi, "A ZVS-PWM three-phase current-fed push-pull DC-DC converter," *IEEE Trans. Ind. Electron.*, vol. PP, no. 99, p. 1, 2012.
- [37] D. Vinnikov, I. Roasto, R. Strzelecki, and M. Adamowicz, "Step-up DC/DC converters with cascaded Quasi-Z-Source network," *IEEE Trans. Ind. Electron.*, vol. 59, no. 10, pp. 3727–3736, oct. 2012.
- [38] W. Li, L. Fan, Y. Zhao, X. He, D. Xu, and B. Wu, "High-step-up and high-efficiency fuel-cell power-generation system with active-clamp flyback-forward converter," *IEEE Trans. Ind. Electron.*, vol. 59, no. 1, pp. 599–610, jan. 2012.
- [39] U. Prasanna and A. Rathore, "Extended range ZVS active-clamped current-fed full-bridge isolated Dc/Dc converter for fuel cell applications: Analysis, design and experimental results," *IEEE Trans. Ind. Electron.*, vol. PP, no. 99, p. 1, 2012.
- [40] F. Rossi, A. Lendasse, D. Francois, V. Wertz, and M. Verleysen, "Mutual information for the selection of relevant variables in spectrometric nonlinear modelling," *Chemometrics and Intelligent Laboratory Systems*, vol. 80, pp. 215–226, 2006.
- [41] Ballard Power Systems Inc., *Introduction to Fuel Cell Technology*, Ballard Power Systems Inc., 2002.
- [42] A. Kraskov, H. Stögbauer, and P. Grassberger, "Estimating mutual information," *Phys. Rev. E*, vol. 69, p. 066138, Jun 2004.
- [43] E. Schaffernicht, R. Kaltenhaeuser, S. S. Verma, and H.-M. Gross, "On estimating mutual information for feature selection," in *Proceedings of the 20th international conference on Artificial neural networks: Part I*, ser. ICANN'10. Berlin, Heidelberg: Springer-Verlag, 2010, pp. 362–367.
- [44] S. Harald, K. Alexander, A. Sergey, and G. Peter, "Least dependent component analysis based on mutual information," *Phys. Rev. E*, vol. 70, p. 066123, 2004.
- [45] I. Staffell and R. Green, "The cost of domestic fuel cell micro-chp systems," *International Journal of Hydrogen Energy*, vol. 38, no. 2, pp. 1088–1102, 2013.